

Direct nanoscale imaging of ballistic and diffusive thermal transport in graphene nanostructures

O.V. Kolosov*, M. E. Pumarol*, P. Tovee*, M. C. Rosamond**, M. C. Petty**, D. A. Zeze**, V. Falco*

* Physics Department, Lancaster University, Lancaster,

LA1 4YB, UK o.kolosov@lancaster.ac.uk, www.nano-science.com

** School of Engineering & Computing Sciences, Durham University, Durham DH1 3LE, UK

ABSTRACT

The list of graphene properties showing potential for nano-electronics applications includes high carrier mobility, superior mechanical strength, and high thermal conductivity [1]. With the mean-free-path (MFP) of thermal phonons at room temperature in graphene on the order of 700 nm and modern semiconductor devices having features on the order of few tens of nm, it is apparent that the ballistic regime must play a significant role in the thermal transport in such nanodevices. Whereas extraordinary thermal properties of graphene suggest its use for heat management, graphene behaviour in such structures is to a great degree unexplored due to lack of suitable methods. Experimentally, so far these phenomena were studied using micro-Raman spectroscopy with lateral resolution inevitably restricted by the optical wavelength to the range of 0.5 - 1 μm [2, 3].

In our study we addressed the challenge of exploration of thermal phenomena in graphene nanostructures by using nanoscale scanning thermal probe [4] in high vacuum (HV) environment (Fig. 1) that allowed us to directly map thermal transport in suspended and supported graphene layers with nanoscale resolution, and to explore both ballistic and diffusive regimes of heat transfer.

Keywords: scanning thermal microscopy, SThM, graphene, heat transport, SPM.

1 SCANNING THERMAL MICROSCOPY (STHM)

1.1 Experimental setup

The thermal sensor (Anasys, SThM probe) was calibrated by linking its resistance to sensor ambient temperature (using small applied voltage so that self-heating is negligible), then the increasing voltage was applied to the sensor and the temperature of Joule self-heating of the sensor was measured as a function of applied power. Finally, the tip of a SThM sensor was brought in contact and out of contact with the sample (in air and in high vacuum environments), while measuring its temperature. That allowed us to quantify heat transfer from the sensor to the sample and to air. An additional experimental setup allowed dynamic measurements of the transient response of SThM probes and to compare it to the

simulation results, which allowed further validation quantitative of the sensor model.

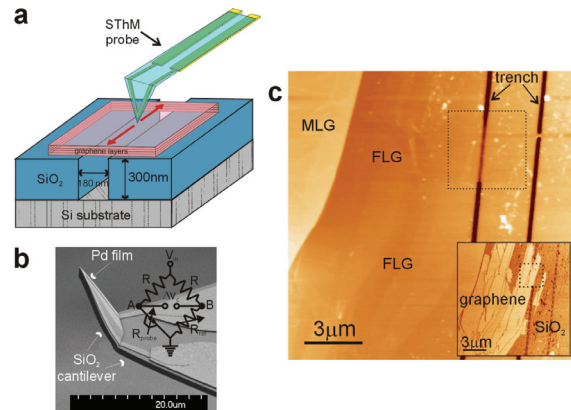


Figure 1 (a) Schematic diagram of the graphene sample on trench substrate, with SThM tip in a typical experimental configuration.

(b) SEM image of the SThM probe (courtesy of Anasys Instruments); embedded, a schematic diagram of the circuitry used for heating and temperature measurement of the nanoscale SThM probe. The driving signal V_{in} is a composite DC (heating) + AC (temperature probing) signal.

(c) AFM topography scan showing the different heights of the graphene layers. The main body of the flake was about 17 atomic layers thick, with few-layer regions (from SLG up to 5-layer FLG) to the right side of the flake. An area of interest of a suspended BLG sheet is enclosed in the dotted square. The inset shows a friction force map of the same area, that allowed to clearly identify graphene and silicon oxide surfaces during SThM measurements owing to clear difference between these areas in friction contrast.

The experimental setup was based on high vacuum multifunctional SPM (HV NT-MDT Solver HV-AFM) encased in a dedicated chamber that can be either evacuated to approximately 10^{-7} torr or used at an ambient air pressure. This chamber was equipped with instrumental feedthroughs for the thermal probe. The SPM was suspended on springs with efficient eddy-current magnetic dampers; during vacuum operation the turbo-molecular pump with an oil-free scroll backing pump provided initial

high vacuum, and the vibrations-free ion pump securing necessary vacuum during thermal measurements. The SPM system used a laser beam deflection system in order to measure forces acting on the SThM in contact mode, and allowed us to position the sensor in contact and out of contact with the test sample, as well as to monitor the force acting between the sample and the probe tip. In the electrical measurement setup the sensor was either a part of a voltage divider in series with the fixed resistor, or a part of an AC-DC electric bridge. In both cases the voltage excitation was provided by the precision function generator (Keithley 3390 50 MHz arbitrary waveform generator). In voltage divider mode a dedicated multimeter (Agilent 34401A 6.5 digits precision) in the ratiometric mode allowed us to measure the resistance of the probe as a function of the voltage at the probe (and, therefore, its temperature due to Joule heating). The probe temperature due to self-heating could be raised in excess of 100 °C above ambient temperature. In the AC-DC bridge configuration, the bridge was balanced at room temperature and absence of SPM laser illumination (we measured that SPM laser deflection monitoring system provided additional heating of approximately 7^o C in air to 15^o C in vacuum), using variable resistor and capacitor.

1.2 Calibration of the nanoscale thermal probe

The thermal calibration of the probes was performed using a temperature stabilized Peltier hot/cold plate (Torrey Pines Scientific, Echo Therm model IC20) at several temperatures from room temperature to 100^oC. As this calibration took place outside the SPM, where there was no heating from the laser. The self-heating of the probe was measured using the same setup. It should be noted that during self-heating, the distribution of the temperature over the probe is inhomogeneous. It should be noted that one has to account for the effect of the laser illumination on thermal measurements. Such illumination increases the tip temperature, and, therefore, its resistance, which was clearly seen in our measurements and we have used reference measurements to account for these phenomena.

2 THEORETICAL ANALYSIS OF NANOSCALE THERMAL PROBING

2.1 Diffusive and ballistic heat transfer

Given complex 3D geometry of these probes, heterogeneity of the probe materials, thermal effects of surrounding media and the sample, and distributed heat generation and sensing element, the most appropriate method to describes functioning of such probes should include 3D modelling of all thermal and electrical phenomena. The electrical transport given scale of the heating elements is on the order from 500-1000 nm and their thickness of 100-1000 nm can be adequately described

by the Ohm's law. The thermal transport in most elements of these probes (with characteristic dimensions on the order of ~um) given MFP for heat transport by phonons in insulating parts of the probe (and corresponding length for electrons in metallic parts of the probe) ranging from low 10s of nm in oxides and nitrides to ~100 nm in single crystalline Si, can be described by diffusive heat transfer equation

$$\rho C_p \frac{\partial T}{\partial t} - \nabla(k \nabla T) = Q \quad (1)$$

where ρ is the density of material, C_p is the heat capacity, k the thermal conductivity and Q the heat source.

The main area where deviations from the diffusive heat transport should be considered is the a) very end of the probe tip and b) probe-surface contact for high thermal conductivity samples with large MFP (i.e. non-metals) where ballistic heat transport can be significant [5-7]. The SiO₂ end of the probe have the effective MFP on the order of $\Lambda_{SiO_2} \approx 10$ nm and 50 nm probe end and therefore Knudsen number for heat transfer $Kn \approx 0.2$. As described in [6], the thermal conductivity in the transition diffusion-ballistic regime k_{db} can be with good approximation estimated as the decrease of the effective heat conductivity k , with

$$k_{db} = \frac{k}{2(\pi Kn)^2} \left[\sqrt{1 + (2\pi Kn)^2} - 1 \right] \quad (2)$$

and corresponding increase in total thermal resistance of tip-surface contact R_c [21] to

$$R_c = \frac{1}{2kL} \left[1 + \frac{8}{3\pi} Kn \right] \quad (3)$$

Low Knudsen numbers $Kn \ll 1$ in (2) correspond to the diffusive transport with $k_{db} \approx k$ and high $Kn \gg 1$ correspond to ballistic transport with $k_{db} \approx k/(\pi Kn)$. Clearly, our probe with Knudsen number $Kn \approx 0.2$ is well described by the diffusive heat transfer.

Clearly, for insulating single crystalline materials of very high thermal conductivity, e.g. diamond, Si, sapphire and graphene layers the heat transport on the material side is ballistic in the vicinity of the ~50 nm contact area, and in this case, the appropriate consideration of modification of thermal resistance using equations (2) and (3) and our SThM measurements will generally provide lower values of thermal conductivity with the factor of $1/(\pi Kn)$.

A. FEA modelling of nanoscale thermal probe

In order to analyse the detail performance of these probes, we first used finite elements analysis (FEA) approach based on COMSOL Multiphysics® to create a realistic three dimensional (3D) model of thermal transport in the probes. This included joule heating of the probe and a temperature dependent resistance of the thermal resistive sensor, exploring ability of such sensors to both generate and evaluate thermal flow to the sample. We used "AC/DC", "Thermal" and "MEMS" modules of COMSOL®, both in static and time dependent solver configurations. All models

were created and debugged in vacuum environment, with air environment subsequently introduced as a block of air enclosing the entire cantilever and the sample with typical results presented in Figure 2.

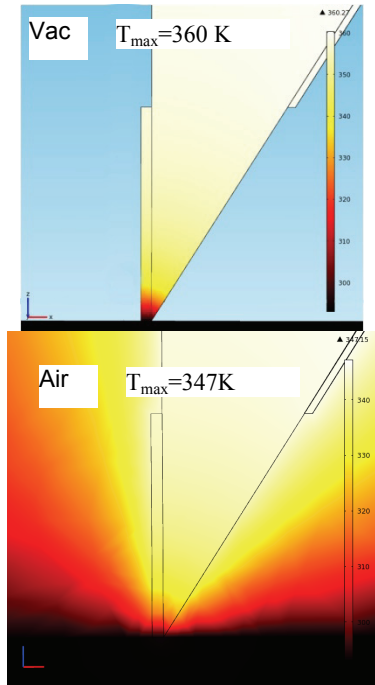


Figure 2: 3D simulation of thermal response of nanoscale probe in contact with Si sample vacuum (top) and in air (bottom image). The temperature drop occurs at the very end of the probe with the temperature increase of the sample with high thermal conductivity (Si) is generally small and is negligible outside the area of immediate contact.

3 NANOSCALE RESOLUTION SCANNING THERMAL MICROSCOPY OF GRAPHENE

We were able to reliably compare thermal resistances for single layer graphene (SLG), supported and suspended bi-layer graphene (BLG) and higher number of graphene layers. SThM maps (Fig. 3) show clear differences between the thermal resistance of graphene areas with varying number of graphene layers with the spatial resolution of approximately 50 nm. The increase of number of supported graphene layers (from SLG through 3-layer (3L) and few layer graphene) lead to clear decrease in heat resistance. Absolute values of total contact thermal resistances R_C , for SLG, BLG, and a trench area with suspended BLG are estimated as, respectively, $R_C(\text{SLG}) = 3.35 \times 10^6 \pm 3 \times 10^4$ K/W, $R_C(\text{BLG}) = 3.15 \times 10^6 \pm 3 \times 10^4$ K/W, and $R_C(\text{BLG-trench}) = 2.75 \times 10^6 \pm 3 \times 10^4$ K/W.

4 THERMAL CONDUCTANCE OF SUSPENDED GRAPHENE LAYERS

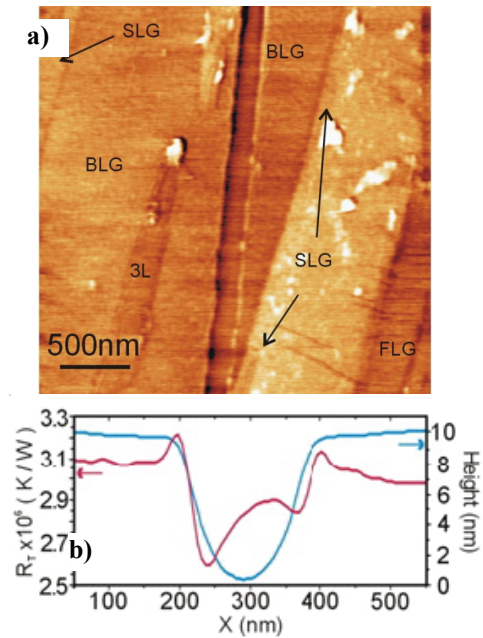


Figure 3: Imaging of heat transport in suspended graphene. (a) SThM thermal image (SThM map) of a zoom-in of graphene sample (dotted square in Fig. 1c) at a constant heating power. Lighter colour corresponds to higher temperature of the probe, and, correspondingly, a higher thermal resistance of the contact and a lower local heat conductance of the sample; the span of thermal contrast on the images corresponds to a probe temperature change of 0.40 C. (b) Topography profile (blue curve, right axis) and averaged thermal resistance profile (red curve, left axis) of bi-layer graphene suspended over the trench. Lower thermal resistance indicates an increase of the heat conductance of graphene with ballistic thermal phonons propagating from the area of the contact along the trench and towards edges of the trench..

Another key observation was that the thermal conductance of BLG layer suspended over trench exceeded that of BLG resting on substrate (darker SThM contrast of the suspended area in Fig. 3a, SThM profiles in Fig. 3b). That finding, initially counterintuitive, suggested that a reduction of lateral heat transport in the graphene layer due to contact with substrate has a prevailing effect. Therefore, we directly explore thermal transport in graphene on a different length scale (50 nm spatial resolution in our SThM measurements vs 500 – 1000 nm in Raman measurements) and, correspondingly, in both ballistic and diffusive regimes of heat transfer in such systems.

5 CONCLUSIONS

In conclusion, we have explored thermal transport in single to few-layer graphene using nanoscale thermal probe with true nanoscale resolution of few tens of nanometres. We have observed higher thermal conductance in the 180 nm wide suspended graphene sheet, compared to the same sheet resting on the substrate and directly imaged spatial distribution of heat transport in graphene nanostructures. We believe that this advancement opens new grounds for nanoscale exploration of heat transport and heat management in graphene-based and other nanoelectronic devices.

REFERENCES

- [1] , K. S.; Geim, A. K.; Morozov, S. V.; Jiang, D.; Zhang, Y.; Dubonos, S. V.; Grigorieva, I. V.; Firsov, A. A. *Science* 2004, 306, (5696), 666-669.
- [2] Balandin, A. A.; Ghosh, S.; Bao, W.; Calizo, I.; Teweldebrhan, D.; Miao, F.; Lau, C. N. *Nano Letters* 2008, 8, (3), 902-907.
- [3] Cai, W.; Moore, A. L.; Zhu, Y.; Li, X.; Chen, S.; Shi, L.; Ruoff, R. S. *Nano Letters* 2010, 10, (5), 1645-1651.
- [4] P. Tovee, M. Pumarol, D. Zeze, K. Kjoller, O. Kolosov, Nanoscale spatial resolution probes for Scanning Thermal Microscopy of solid state materials, <http://arxiv.org/abs/1110.6055>
- [5] Prasher, R., Predicting the thermal resistance of nanosized constrictions. *Nano Letters*, 2005. 5(11): p. 2155-2159.
- [6] Ordonez-Miranda, J., R.G. Yang, and J.J. Alvarado-Gil, A constitutive equation for nano-to-macro-scale heat conduction based on the Boltzmann transport equation. *Journal of Applied Physics*, 2011. 109(8): p. 8.
- [7] Chen, G., Ballistic-Diffusive Heat-Conduction Equations. *Physical Review Letters*, 2001. 86(11): p. 2297-2300.